This is an Accepted Manuscript of an article published by Taylor & Francis in Nuclear Technology on June 12, 2024, available at: https://doi.org/10.1080/00295450.2024.2348849.

Title: Electrochemical Identification of Metal Chlorides in Eutectic LiCl-KCl Without Prior Knowledge of Analyte Identities

Author Names: Tyler Williams[1,z], Jason Torrie[1], Mark Schvaneveldt[1,2], Ranon Fuller[1], Greg Chipman[1,3], Devin Rappleye[1]

Affiliations

[1]Department of Chemical Engineering, Brigham Young University, Provo, UT, 84602, USA

[2]Present Address: Argonne National Laboratory, Lemont, IL, 60439, USA

[3]Present Address: Savannah River National Laboratory, Jackson, SC, 29831, USA

[z] Corresponding Author: wtylerb@byu.edu

Abstract

The identities of unknown analytes within four eutectic LiCl-KCl melts were determined using electrochemical methods, simulating the uncertainty of electrochemically probing an electrorefiner salt bath or molten salt nuclear reactor. With a variety of electrochemical methods (e.g., cyclic voltammetry, chronopotentiometry, square-wave voltammetry) and electroanalytical techniques (e.g., semi-differentiation), every analyte was positively identified, although one false positive occurred due to an unexpected chemical interaction. This study highlights some remaining challenges for the use of electrochemical sensors in nuclear material control and accountability in molten salts: (1) quantification of analytes without the use of calibration curves (e.g., error in property values, such as diffusion coefficient) and (2) additional and interfering electrochemical signals due to interaction and alloying of multiple species.

Keywords: Voltammetry, Material Control and Accountability, Nuclear Safeguards, Molten Salt

1. Introduction

The international and domestic development of nuclear safeguards and material control and accountability (MC&A) tools for advanced nuclear reactors and fuel cycles becomes more urgent as nuclear technology expands throughout the world and closed fuel cycles become more prevalent [1,2]. Safeguards and MC&A tools will include sensors that are optimized for detecting and quantifying special nuclear material in fuel cycle processes. Molten salt media are common in advanced reactor designs and fuel cycle processes [3–5]. Hence, there is significant interest and effort in developing electrochemical sensors that are optimized for molten salt processes such as electrorefiners (ERs) and molten salt reactors (MSRs). With current developments of ERs [6] and MSRs [7,8] throughout the world, now is the time to prepare sensor technology that can ensure that these processes are safeguarded and monitored well.

Electrochemical sensors are well-suited to ERs and MSRs because of their resistance to thermal, corrosive, and radiative damage. These sensors have been demonstrated in many prior studies, but almost always in situations where experimentalists had some prior knowledge of their systems, including the identity of analytes that were studied [5]. The standard method is to prepare a solution with a known quantity of an analyte (or analytes), measure the concentration with electrochemical methods, measure the concentration of analytes with another analytical method (e.g., ICP-MS), build a calibration curve, and then test that calibration curve on several additional data points [5,9–11]. Because prior knowledge influences decisions, this method may lead to an overestimation of a technique's analytical utility and accuracy [12]. This paper's purpose is to investigate the ability of electrochemical methods to identify unknown analytes in the absence of process knowledge and constraints (i.e., any soluble electroactive species is possible).

2. Methods

This paper outlines the collection and analysis of electrochemical data for 4 systems that were prepared without an experimentalist's knowledge. However, the following information was available for each prepared system to the experimentalist: (1) the base salt composition (eutectic LiCl-KCl); (2) melt

temperature (773 ± 1 K); (3) the working electrode (WE) material (tungsten, W) and diameter (1.5 mm); (4) the counter electrode (CE), quasi-reference electrode (qRE) material (W), and diameters (1.5 mm); (5) the non-radioactive nature of surrogate analyte(s); and (6) an upper concentration limit for the unknown analyte(s) (i.e., less than 3 wt% to maintain diffusion dominated mass transfer). The experimentalist did not know the color nor the source of the salt. Molten salt solutions were prepared from salts either already in the lab inventory or purchased from a vendor so that the experimentalists could not infer the identity based on their prior knowledge of the lab's chemical inventory.

2.1 Experimental Preparation and Equipment. Experiments were conducted in a glovebox under Ar atmosphere (LC Technology Solutions, LC-300-DS) with H_2O and O_2 levels maintained at <1 ppm and <10 ppm, respectively. LiCl (>99%, Alfa Aesar, 36217) and KCl (>99%, Alfa Aesar, 11595) were dried overnight in a vacuum oven at 480 K, then fused in a lab-modified tube furnace (MTI, OTF-1200X-S-NT) in eutectic proportions at 900 K for 1 hr and subsequently cooled in the glovebox. Analytes were added to the previously fused eutectic, heated to 773 K in alumina crucibles (Advalue Tech, AL-2100), and held at that temperature for at least 30 min before electrochemical measurements were made. The alumina crucibles had previously been dried in a vacuum oven overnight at 503 K and then held at 1173 K for 2 hrs in a tube furnace within the glovebox. The electrochemical cell was shielded from induction currents originating in the tube furnace's heating coils by a grounded nickel tube. A three-electrode system was used with W rods (99.95%, Alfa-Aesar) for the 1.5 mm WE, qRE and CE. The CE was immersed deeper in the salt than the WE, so that it would not limit the current experienced at the WE. Electrodes were cleaned prior to electrochemical measurements with a light sanding with 220 grit paper, if visual residue was present, followed by polishing with crocus cloth until no residue was visible and W electrodes had an lustrous appearance. The qREs were used for experimental simplicity but required that potentials be referenced to the oxidation potential of Cl^- to Cl_2 or the reduction potential of Li^+ to Li. These electrodes were controlled using an Autolab potentiostat (PGSTAT302N) and NOVA 2.1 software. The analytes that were prepared can be found in Table 1. They were not known to the experimentalist

performing the measurement and included $MgCl_2$ (Thermo Fisher Scientific, ultra-dry, 99.9%, 42843), VCl_3 (Thermo Fisher Scientific, 99%, 014039), $CrCl_3$ (Thermo Fisher Scientific, anhydrous, 99.9%, 035691), $SmCl_3$ (Thermo Fisher Scientific, ultra-dry, 99.9%, 035804), $LaCl_3$ (Thermo Fisher Scientific, ultra-dry, 99.9%, 035702), and $FeCl_2$ (Thermo Fisher Scientific, ultra dry, 99.99%, 035701). Except for System 4, analytes were selected at random with no specific application to minimize the experimentalist ability to deduce an answer based on reasoning (i.e., expecting only "relevant" salts, such as actinide and lanthanide chlorides). System 4 analytes were selected as a simple simulant of eutectic LiCl-KCl bearing a lanthanide chloride with steel corrosion products present. However, the rationale for system 4 was not known to the experimentalist beforehand.

Table 1. Analyte identities and concentrations for each experiment.

System	Analyte Identity	Analyte Concentration / wt%
1	$MgCl_2$	0.708
2	VCl_3	2.66
3	$SmCl_3$	0.71
4	$LaCl_3$, $CrCl_3$, $FeCl_2$	0.998, 0.291, 0.533

2.2 General Electroanalytical Procedure. Experimental procedures were set as follows and could be augmented with additional measurements, as the experimentalist deemed to be appropriate. After establishing electrochemical contact between all three electrodes and the molten solution, electrochemical impedance spectroscopy (EIS) at the open-circuit potential (E_{OCP}) was used to measure the uncompensated solution resistance (R_s). The R_s value was taken to be the x-intercept of a Nyquist plot at a frequency around 10-100 kHz. Following EIS, a positive feedback test was conducted on a potential step while *iR* compensating at 85-90% of R_s to verify that the potentiostat was able to control potential set-point changes within the required time intervals for common cyclic voltammetry (CV) and square-wave

voltammetry (SWV) scan rates. 100% compensation was not used because this leads to poor control of the potential due to instabilities in the electronic feedback loop (i.e., ringing). Once the optimal compensation percentage was determined, it was used during all potential-controlled measurements (e.g., CV, SWV).

Next, the full electrochemical window (i.e., the potential range extending from the reduction to the oxidation of the base solution – about 3.6 V in LiCl-KCl [13,14]) was investigated with CV. Because a qRE was used, this step is required to reference the potential of an unknown reaction to the potential of a known reaction like Cl_2 evolution or Li^+ reduction. CV was next conducted with varying scan rates and potential ranges to investigate the qualitative behavior of the reactions occurring in the solution. For example, the interdependencies of peaks could be observed by changing the upper and/or lower limits of CV scans. With this data, reactions could also be classified by the shape of their peaks: "duck-shaped" peaks for reversible reactions with soluble products and reactants (soluble-soluble); sharp, symmetric peaks for reactions with surface-constrained reactants and products (e.g., alloying); sudden reduction peaks dwarfed by their corresponding oxidation peaks, which drop abruptly, for reactions with soluble reactants and surface-constrained products (soluble-insoluble); "hockey-stick-shaped" reductions or oxidations where no peak is formed and the current rises or falls precipitously for reactions whose reactants are the solution (LiCl-KCl) itself. In a pure LiCl-KCl bath with no analytes present, one would expect to see a low current baseline (not zero due to capacitance at the electrode/solution boundary) with hockey-stick reductions or oxidations separated by around 3.6 V. The reduction of Li^+ may have an associated large oxidation peak for when the Li metal is oxidized and dissolved back into the solution, while the oxidation of Cl^- may or may not have a reduction peak because Cl_2 may dissolve into the salt away from the electrode or bubble out of solution.

Next at least five *iR*-compensated square-wave voltammetry (SWV) scans with frequencies (*f*) from 1 to 50 Hz on peaks of interest to measure the number of electrons *n* exchanged using [15]:

This is an Accepted Manuscript of an article published by Taylor & Francis in Nuclear Technology on June 12, 2024, available at: https://doi.org/10.1080/00295450.2024.2348849.

$$w \approx 3.53\frac{RT}{nF} \quad (1)$$

$$w_2 \approx 0.91\frac{RT}{nF} \quad (2)$$

for soluble-soluble or soluble-insoluble reactions, respectively. Where w is the width of a SWV peak at half its height, w_2 is the back (more negative, if reducing) half of w, R is the universal gas constant, T is temperature, n is the stoichiometric number of exchanged electrons, and F is Faraday's constant.

Next, the formal potential ($E^{0'}$) for the reaction was estimated from the potential plateaus of chronopotentiometry (CP) followed by open-circuit potentiometry (OCP). The principle is that when current is controlled (non-zero current for CP, zero current for OCP), potential plateaus with time indicate that there is a reaction occurring at that potential that can satisfy the demands of current made by the electrochemical workstation. The average potential of this plateau is then taken and assumed to be approximately $E^{0'}$. For more accurate estimations of $E_j^{0'}$, approximate concentrations of the reactants and products were calculated using an estimated diffusion coefficient of 10^{-5} cm^2 s^{-1} and the following CV relations for soluble-soluble or soluble-insoluble reactions, respectively [16–18]:

$$i_p = 0.4463AC_O^*\sqrt{\frac{(nF)^3 D_O \nu}{RT}} \quad (3)$$

$$i_p = 0.6105AC_O^*\sqrt{\frac{(nF)^3 D_O \nu}{RT}} \quad (4)$$

where i_p is the peak current, A is the WE surface area, C_o^* is the bulk concentration of the oxidized species O, D_O is the diffusion coefficient of species O, and v is the scan rate. Note that Equations 3 and 4 can also be applied to the reduced species (R) using C_R* and D_R, if the reduced species is present in the salt rather than the oxidized species. These estimated concentrations were then used to calculate $E^{0'}$ from the OCP using the Nernst Equation [19]:

$$E = E^{0\prime} + \frac{RT}{nF} ln\left(\frac{C_O^*}{a_R}\right) \quad (5)$$

This is an Accepted Manuscript of an article published by Taylor & Francis in Nuclear Technology on June 12, 2024, available at: https://doi.org/10.1080/00295450.2024.2348849.

where a_R is the activity of the reduced species which is assumed to be 1 for a metal deposit or the bulk concentration of the reduced species (C_R*) for a soluble species. Now, with estimations of n and $E^{0'}$ for each reaction in the solutions, the identity of the unknown analyte(s) could be guessed by comparison to electromotive force (EMF) tables (see Table 2).

Table 2. Reproduction of Plambeck's EMF series based on molar concentrations, shifted to the Cl^-/Cl_2 and Li^+/Li references. Reprinted (adapted) with permission from [13]. Copyright 1967 American Chemical Society.

Couple	$E_j^{0'}$ / **(V vs Li^+/Li)**	$E_j^{0'}$ / **(V vs Cl_2/Cl^-)**	**Couple**	$E_j^{0'}$ / **(V vs Li^+/Li)**	$E_j^{0'}$ / **(V vs Cl_2/Cl^-)**
Li(I)-Li(0)	0	-3.626	Ga(III)-Ga(0)	2.464	-1.162
La(III)-La(0)	0.427	-3.199	In(III)-In(0)	2.504	-1.122
Nd(III)-Nd(0)	0.485	-3.141	Ni(II)-Ni(0)	2.509	-1.117
Gd(III)-Gd(0)	0.516	-3.11	V(III)-V(0)	2.544	-1.082
Mg(II)-Mg(0)	0.724	-2.902	V(III)-V(II)	2.556	-1.07
Zr(IV)-Zr(II)	1.44	-2.186	Ag(I)-Ag(0)	2.561	-1.065
Mn(II)-Mn(0)	1.455	-2.171	Cr(III)-Cr(0)	2.654	-0.972
Zr(IV)-Zr(0)	1.497	-2.129	Sb(III)-Sb(0)	2.669	-0.957
Al(III)-Al(0)	1.542	-2.084	Bi(III)-Bi(0)	2.669	-0.957
Zr(II)-Zr(0)	1.554	-2.072	Mo(III)-Mo(0)	2.701	-0.925
Ti(II)-Ti(0)	1.564	-2.062	Cr(III)-Cr(II)	2.779	-0.847
Ti(III)-Ti(0)	1.704	-1.922	Cu(II)-Cu(0)	2.856	-0.77
Zn(II)-Zn(0)	1.738	-1.888	Fe(III)-Fe(0)	2.942	-0.684
V(II)-V(0)	1.771	-1.855	Pd(II)-Pd(0)	3.09	-0.536
Ti(III)-Ti(II)	1.984	-1.642	Rh(III)-Rh(0)	3.108	-0.518
Cr(II)-Cr(0)	1.879	-1.747	Ir(III)—lr(0)	3.247	-0.379
Cd(II)-Cd(0)	1.988	-1.638	Pt(II)-Pt(0)	3.304	-0.322
Fe(II)-Fe(0)	2.132	-1.494	Cu(II)-Cu(I)	3.365	-0.261
Pb(II)-Pb(0)	2.203	-1.423	Fe(III)-Fe(II)	3.39	-0.236
Sn(II)-Sn(0)	2.222	-1.404	Au(I)-Au(0)	3.509	-0.117
Co(II)-Co(0)	2.313	-1.313	Cl_2-Cl^-	3.626	0
Cu(I)-Cu(0)	2.347	-1.279			

In most cases, the preceding methods were sufficient to identify the analyte(s) in the solution. However, when CV peaks overlapped, an analytical method known as semi-differentiation, or convolution, was used to separate signals into distinct peaks. These semi-differentiated peaks were analyzed with the following relations:

This is an Accepted Manuscript of an article published by Taylor & Francis in Nuclear Technology on June 12, 2024, available at: https://doi.org/10.1080/00295450.2024.2348849.

$$e(t) = -\frac{n^2F^2AC_O^*\nu}{4RT}D_O^{1/2}sech^2\left(\frac{nF}{2RT}\left(E(t) - E_{1/2}\right)\right) \quad (6)$$

$$e\left(E_{1/2}\right) = -\frac{n^2F^2AC_O^*\nu D_O^{1/2}}{4RT} \quad (7)$$

for soluble-soluble reactions [20], where *e* is the semi-derivative of current (*i)* with respect to time (*t*), and $E_{1/2}$ is the half-wave potential and

$$e(t) = -\frac{n^2F^2AC_O^*\nu}{RT}D_O^{1/2}exp\left(\frac{nF}{RT}(-\nu t)\right) \quad (8)$$

$$e\left(E_{1/2}\right) = -\frac{n^2F^2AC_O^*\nu D_O^{1/2}}{2RT} \quad (9)$$

$$E_{1/2} = E^{0\prime} + \frac{RT}{nF}ln\left(\frac{C_O^*}{2C^0}\right) \quad (10)$$

for soluble-insoluble reactions [21,22]. With these relations, peaks separated by semi-differentiated could be analyzed in the same manner as typical CV peaks.

Analyte identification was the main purpose of this analysis, but roughly quantifying the unknown analyte to an order of magnitude was also of interest. To do so, at least six *iR*-compensated CV scans from 25 to 500 mV s^{-1} were conducted on peaks of interest. Then, additional CV scans were made at several different electrode depths controlled with a vertical translator (Velmex, A2509P10-S2.5-TL, 0.0254 mm precision) to estimate the surface area (*A*). This last method is known as the differential height method and is used to calculate the immersion depth of an electrode by extrapolating the i_p vs depth data to zero current. Then using diffusion coefficients from literature for the now-known species and Equations 3, 4, 6, 7, 8, and 9, C_j could be calculated. It is important to note that these equations are only valid if the reaction is electrochemical reversible for a given scan rate. This was verified by confirming that i_p vs $v^{1/2}$ is linear and E_p, the peak potential, is not dependent on *v*.

Additionally, the potential step size (E_{step}) of the digital staircase in CV was recommended to be less than or equal to 1 mV. Using a small E_{step} value is important because larger E_{step} values in digital

This is an Accepted Manuscript of an article published by Taylor & Francis in Nuclear Technology on June 12, 2024, available at: https://doi.org/10.1080/00295450.2024.2348849.

staircase CV depresses the peak current (i_p) more [23], leading to more underestimated concentrations [24]. The lower switching potential for CV scans was to be 0.1 to 0.2 V less than the peak potential (E_p) for the peak of interest while the upper switching potential was to be far enough to establish a clear baseline for baseline correction, if needed. Equations 3, 4, 6, 7, 8, and 9 typically deliver C_O^* in units of mol cm^{-3} so the following equations were used to convert this value into mol% and wt% respectively:

$$mol\% = 100\left(C_j^*\right)/\left(C_j^* + C_{LiCl-KCl}^*\right) \quad (11)$$

$$wt\% = 100\left(MW_j C_j^*\right)/\left(MW_j C_j^* + MW_{LiCl-KCl} C_{LiCl-KCl}^*\right) \quad (12)$$

$$C_{LiCl-KCl}^* = \frac{\rho_{LiCl-KCl}}{MW_{LiCl-KCl}} \quad (13)$$

where $\rho_{LiCl\text{-}KCl}$ at 773 K is taken to be 1.621 g cm^{-3} [25]. Because the focus of this study was on the identification of unknown analytes, no attempt was made to quantify the analyte with ICP-MS or similar methods. Instead, the prepared concentration was used to roughly evaluate the accuracy of quantification predictions.

3. Results

The results of each identification attempt are given in order of increasingly difficult analysis. Care has been taken to give a somewhat unified methodology for the procedure, but the individual conducting each experiment was responsible for their own measurements and analysis which introduced some variability in methodology. Furthermore, the unique challenges of some experiments required adaptation.

3.1 Solution Resistance and iR-compensation. Once CV scans confirmed that electrodes were situated in the melt, EIS was conducted with a 10 mV$_{RMS}$ amplitude from 100 to 0.01 kHz (save for Experiment 3 where EIS was stopped at 2 kHz) and R_s were measured (see Table 3) and compensated for, leaving a

small level of uncompensated resistance (R_u). This remaining R_u is necessary for electrochemical workstations to prevent ringing (i.e. oscillations) during controlled potential experiments.

Table 3. R_s, iR-compensation, and R_u for each experiment.

Experiment	**Measured R_s / Ω**	***iR*-compensation / Ω**	**R_u / Ω**
1	0.22	0.187	0.033
2	0.35	0.26	0.09
3	0.187	0.159	0.028
4	0.178	0.135	0.043

3.2 System 1 Identification. A full-window, *iR*-compensated CV scan (see Figure 1) was taken of System 1 which revealed four electrochemical reactions. The redox couple for peaks C/C' was classified as a soluble/insoluble due to sharp rise of peak C and the sharp rise and fall of peak C' characteristic of a deposited electroactive species (i.e., metal stripping behavior). A and A' were attributed to the Li/Li^+ redox pair because of the reduction's hockey-stick form. Peaks B and B' were attributed to a surface interaction between the metallic product of peak C and Li because of their sharp, symmetric peaks. Peak D' was attributed to anodic reactions, such as Cl_2 generation. However, the cyclic voltammogram shown in Figure 1 was not extended to sufficiently positive potentials to verify the onset potential for Cl_2 generation. The additional blips in current that can be seen in Figure 1 were attributed to electrical noise (e.g., stray vibrations from surroundings, electromagnetic fields near the cell and electrode lead wires).

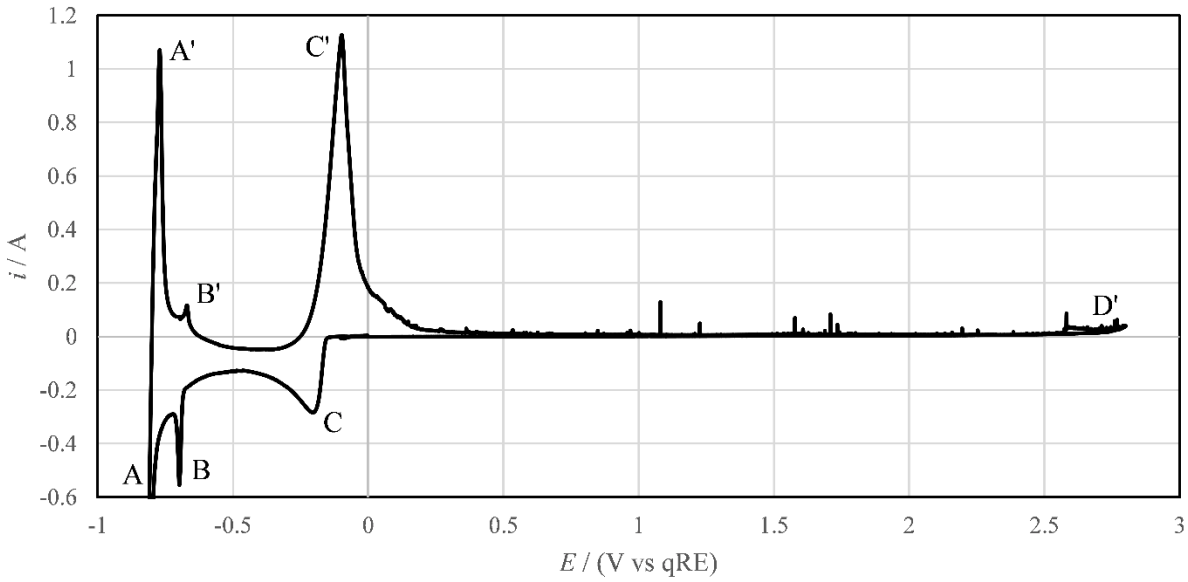

Figure 1. Full-window, *iR*-compensated cyclic voltammogram of System 1. A = 0.694 cm^2, v = 200 mV s^{-1}, E_{step} = 1 mV, R_u = 0.033 Ω.

Next, SWV measurements were conducted to help identify the analyte's oxidation state. SWV scans of the reduction were conducted with f values from 5 to 50 Hz, a step size (ΔE_s) of -4.68 mV, and a square-wave amplitude (ΔE_{sw}) of 47.71 mV. Plugging w_2 vs f data (see Figure 2) into Equation 2 indicated that n = 2.02 ± 0.04 (95% confidence interval). Because this is a metal-deposition reaction, as the cyclic voltammogram shape indicates, the analyte was assumed to be in a +2 oxidation state prior its reduction to metal.

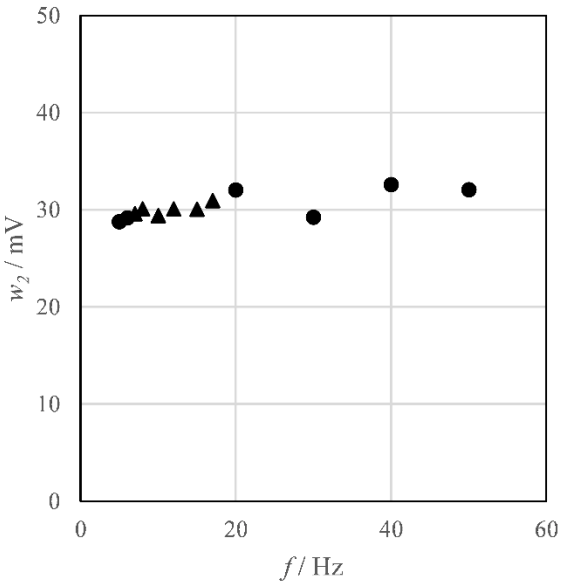

Figure 2. w_2 vs f from iR-compensated square-wave voltammograms of System 1. Analyzed data points are shown as triangles and other data points are shown as circles. A = 0.694 cm^2, ΔE_s = -4.68 mV, ΔE_{sw} = 47.71 mV, R_u = 0.033 Ω.

Then, CP and OCP were used to measure $E^{0'}$ approximately. First, -500 mA was applied for 5 s. Then, OCP was used to observe the transition back to equilibrium. The responses from these measurements can be seen in Figure 3. Based on this data and assuming that $E_{eq} \approx E^{0'}$, $E^{0'}$ was estimated to be 0.68 V vs $E_{Li/Li(I)}{}^{0'}$. With $E^{0'}$, the oxidation state of products and reactants, and Table 2, the analyte was correctly identified as $MgCl_2$.

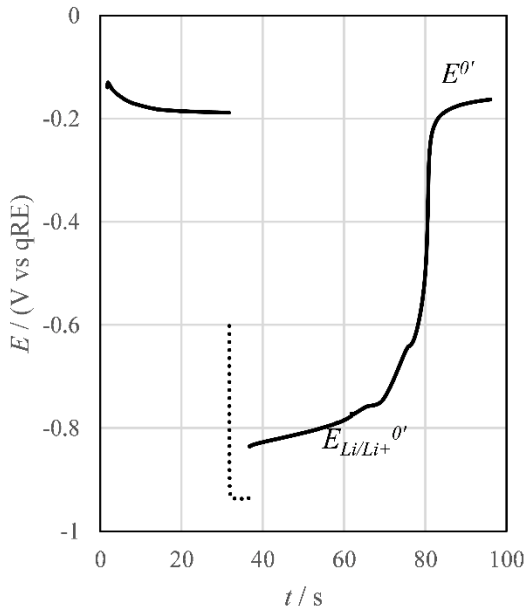

Figure 3. CP at -500 mA (dotted) and OCP (solid) of System 1. A = 0.694 cm^2.

With the analyte identified, an approximate concentration was calculated. An average $D_{Mg(II)}$ value was then estimated to be 1.84 x 10^{-5} cm^2 s^{-1} using the average of the minimum (1.26 x 10^{-5} cm^2 s^{-1}) and maximum (2.42 x 10^{-5} cm^2 s^{-1}) values found in literature [26,27]. CV was used to estimate A and calculate $C_{Mg(II)}^*$ with scans using a step height (E_{step}) of 1 mV. The differential height method estimated that A = 0.694 cm^2. The reaction was verified to be reversible by plotting the peak potential (E_p) and current (i_p) against scan rate (v) and $v^{1/2}$, respectively. As shown in Figure 4, i_p is linear with $v^{1/2}$ and E_p is independent of v. With all this information and Equation 4, the unknown analyte was calculated to be 0.098 ± 0.003 M $MgCl_2$ (0.574 ± 0.018 wt% or 0.336 ± 0.011 mol%). This rough concentration calculation compares well with the 0.708 wt% $MgCl_2$ that was prepared (18.9% error).

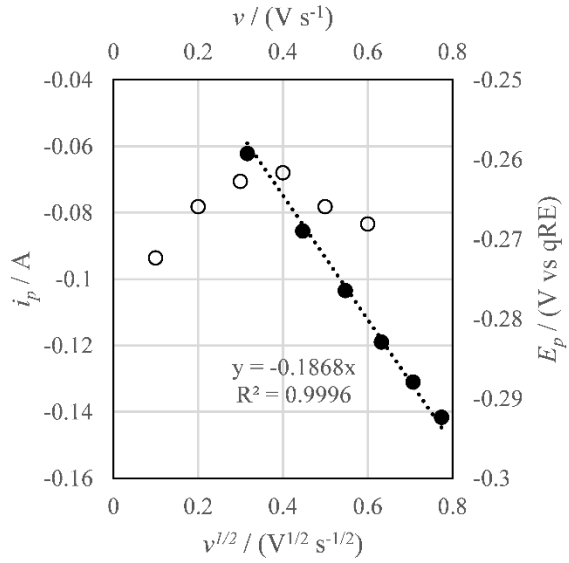

Figure 4. i_p vs $v^{1/2}$ (solid) and E_p vs v (empty) for System 1. A = 0.694 cm^2, E_{step} = 1 mV, R_u = 0.033 Ω.

3.2 System 2 Identification. A full-window, *iR*-compensated CV scan (see Figure 5) was taken of System 2 which revealed six electrochemical reactions. A and A' were attributed to the reduction and oxidation of Li^+ because of the reduction's hockey-stick shape. Based on the location of A and A', $E_{Li/Li^+}^{0'}$ = -2.6 V vs. qRE. F' was attributed to Cl_2 production for the same reason. Peak D' was attributed to a reaction that relied on the products of A and/or F' because it is no longer present when CV scan range is trimmed to exclude peaks A/A' and F/F' (see dotted line in Figure 5). Peaks B and C were classified as two reactions belonging exclusively to the analyte being studied, with B classified as soluble-insoluble (i.e., deposition), and C classified as soluble-soluble. Peak E' was not analyzed because of its small magnitude and lack of a corresponding reduction peak. The small, unlabeled reduction occurring between C and B was not analyzed because it was assumed to belong to the same species responsible for B and C (e.g., adsorption).

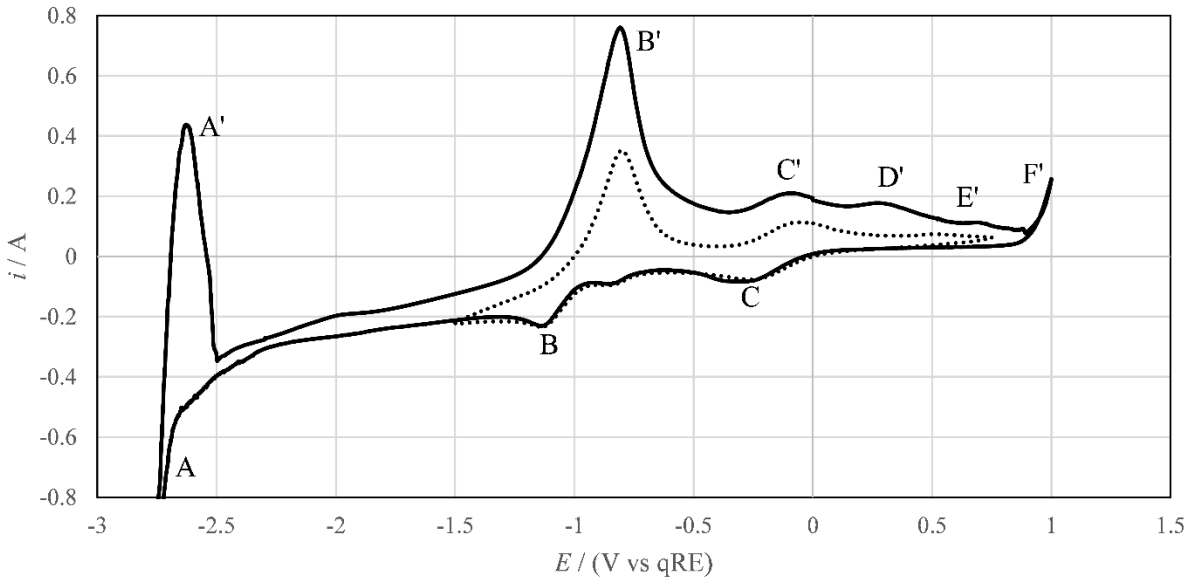

Figure 5. Full-window (solid) and focused (dotted), *iR*-compensated cyclic voltammogram of System 2. A = 1.34 cm^2, v = 300 mV/s, ΔE_{step} = 1 mV, R_u = 0.09 Ω.

Next, SWV scans of both reductions were conducted with f values from 5 to 50 Hz, with ΔE_s = 1 mV and ΔE_{sw} = 10 mV (see Figure 6). Equation 1 was combined with w vs f data to calculate that the soluble-soluble reaction had an n value of 0.98 ± 0.03. Equation 2 and w_2 vs f data were used to calculate that n was 1.01 ± 0.04 for the soluble-insoluble reaction. Upon later reflection, the validity of Equation 2 in this situation is questionable because it was developed under the assumption of semi-infinite diffusion of the oxidized species from the bulk [15,2E]. However, in this scenario, the oxidized species is being generated at the electrode surface as a product of peak C, some of which may be diffusing away from the electrode. This scenario has been shown to differ in its voltametric response from the derived semi-infinite linear diffusion response [29]. No clear oxidation state of the soluble-soluble reactant or product could be assumed with the available information at this time.

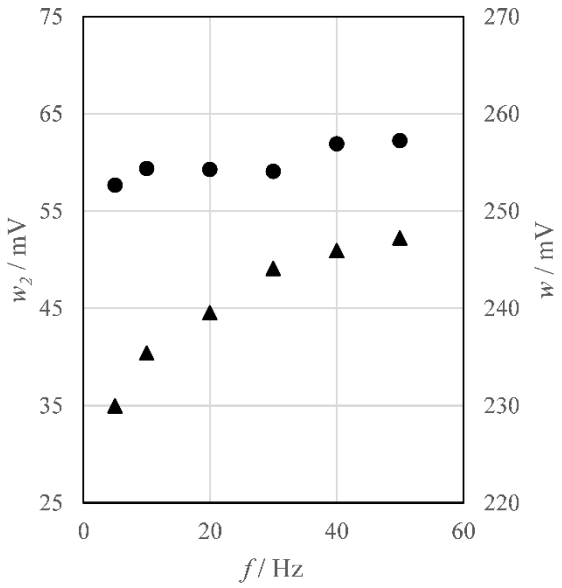

Figure 6. w_2 (circles) vs f and w (triangles) vs f from iR-compensated square-wave voltammograms of the soluble-insoluble peak B (circles) and soluble-soluble peak C (triangles) reactions in System 2, respectively. A = 1.34 cm^2, ΔE_s = 1 mV, ΔE_{sw} = 10 mV, R_u = 0.09 Ω.

Next, CP and OCP (see Figure 7) were used to measure approximate $E^{0'}$ values of -1.8 and -0.96 V vs $E_{Cl\text{-}/Cl2}^{0'}$ (note that Figure 7 is plotted with respect to E_{qRE}). With $E^{0'}$ and the n value for the soluble-soluble reaction, identification was attempted. At first, no analytes seemed to fit the data until it was realized that the n value for the soluble-insoluble reaction could have been faulty if there was a multi-step reduction. With this assumption relaxed, measurements aligned well with both $CrCl_3$ and VCl_3 as being the analyte, but VCl_3 was correctly selected as the unknown analyte after Equation 5 was used to modify the expected potential based on estimated concentrations, as described in Section 2.2.

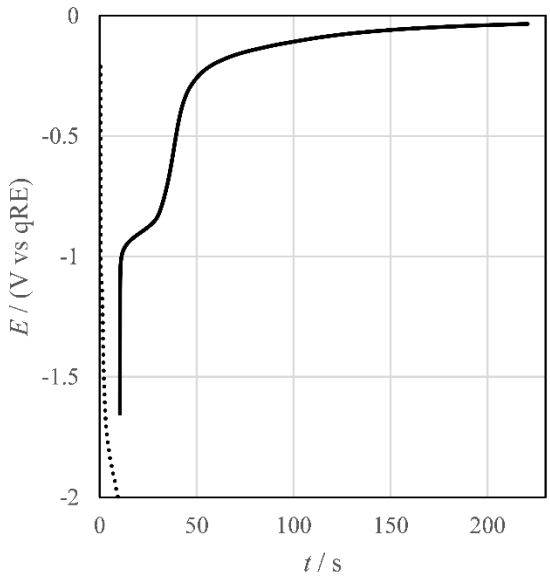

Figure 7. CP at -200 mA (dotted) and OCP (solid) of System 2. A = 1.34 cm^2.

Because the soluble-insoluble reaction seemed to be a multi-step reaction, the soluble-soluble reduction was used exclusively to estimate the concentration. The decision to classify the soluble-insoluble reaction as something other than a reversible, single-step, diffusion-controlled reaction was confirmed by the non-zero intercept of the i_p vs $v^{1/2}$ plot (see Figure 8). CV data was taken with a E_{step} of 1 mV. The soluble-soluble model was assumed to be reversible based on the data in Figure 8. After completing the measurements, the A was approximated to be 1.34 cm^2 by visual inspection of the electrode (a departure from the established methodology by the experimentalist which likely introduced error [30]). With this information, Equation 3, and an average $D_{V(III)}$ value of 7.90 x 10^{-5} cm^2 s^{-1} from literature values [31,32], the unknown analyte was concluded to be 0.040 ± 0.012 M VCl_3 (0.111 ± 0.034 mol% or 0.313 ± 0.097 wt%). This estimation was an order of magnitude off (88.2% error) from the mass that was weighed out before the experiment (2.66 wt%). Error is likely due to poor A estimation and volatility of the analyte.

This is an Accepted Manuscript of an article published by Taylor & Francis in Nuclear Technology on June 12, 2024, available at: https://doi.org/10.1080/00295450.2024.2348849.

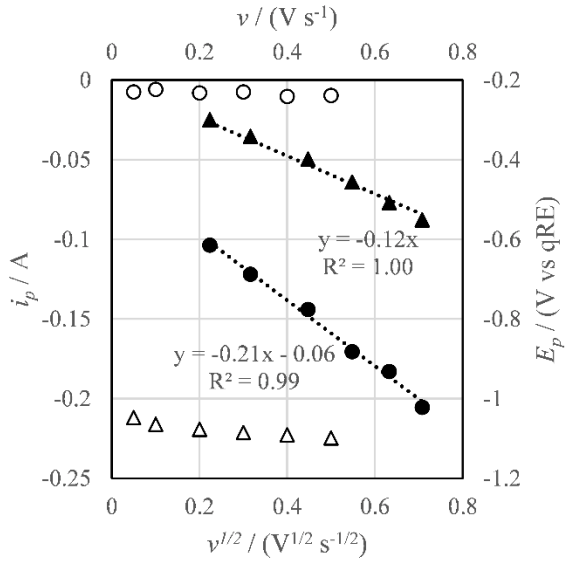

Figure 8. i_p vs $v^{1/2}$ (solid) and E_p vs v (empty) for the soluble-insoluble peak B (circles) and solube-soluble peak C (triangles) reactions in System 2. A = 1.34 cm^2, E_{step} = 1 mV, R_u = 0.09 Ω.

3.4 System 3 Identification. A full-window, *i*R-compensated CV scan (see Figure 9) was taken of System 3 which indicated ~7 electrochemical reactions. This analysis is complicated by the apparent dilute levels of the analyte. At these low of currents, signals from impurities may appear significant relative to the analyte. Peaks D and D' were classified as soluble-soluble reactions belonging to the analyte. Peaks B, B', C, E, and F were not considered because they were inconsistently present or atypical of an electrochemical reaction. For example, no evidence of signals E or C are present in the truncated CV scan (dotted series shows in Figure 9) despite the potentials where E or C occur or commence still being included indicating that they are dependent on or results from interactions in the salt or at the electrode surface (e.g., adsorption). In the case of peaks A/A' and B/B', sharp spikes are typical of electronic instability which could be caused by the compensation for resistance. The electronic feedback loop at the more extreme potentials becomes less stable [33,34]. The sharp rise in current due to Li depositions (see Figures 1 and 5) can destabilize the electronic control loop used for resistance compensation at certain time scales. However, A and A' were attributed to Li^+ reduction and Li oxidation

based on its position relative to peaks G/G' and the known potential window for LiCl-KCl of ~3.6 V. G and G' were attributed to Cl^- oxidation and reduction.

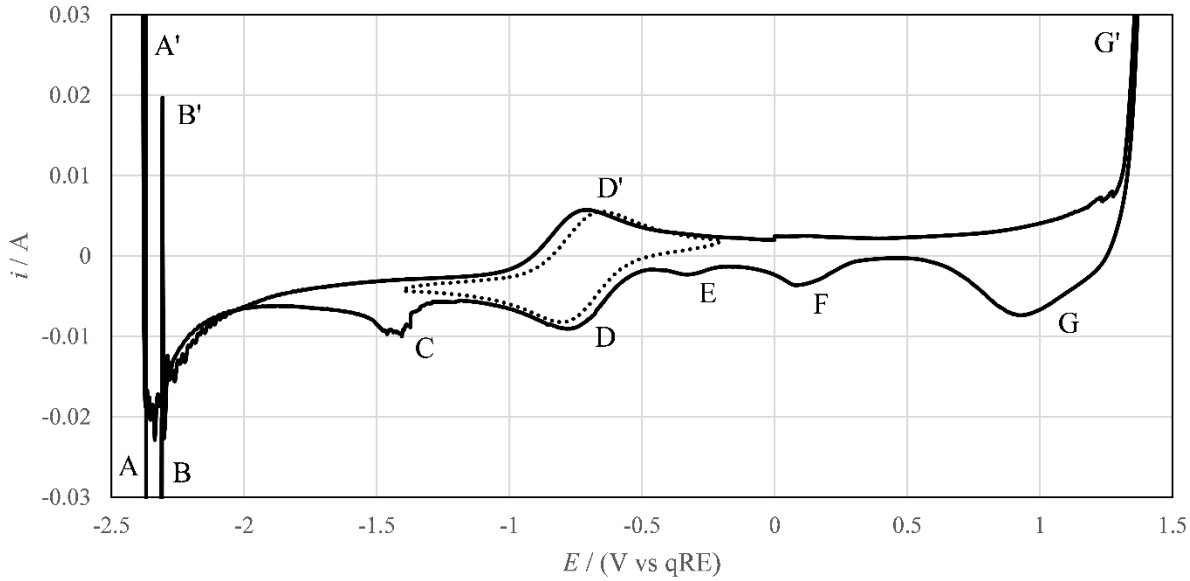

Figure 9. Full-window, *iR*-compensated cyclic voltammogram of System 3. A = 0.718 cm^2, v = 200 mV s^{-1}, E_{step} = 1 mV, R_u = 0.028 Ω.

Next, SWV was used to identify n for the reaction. Scans were taken with f values from 1 to 50 Hz, ΔE_s = 5 mV, and ΔE_{sw} = 20 mV (see Figure 10). Equation 1 was then used to calculate that n = 0.99 ± 0.04. $E^{0'}$ was approximated by averaging the E_p values for D and D', resulting in a value of approximately 1.66 V vs $E_{Li/Li(I)}{}^{0'}$. Based on this $E^{0'}$ value and the lack of other significant peaks within the potential window, the reaction was assumed to be Sm^{2+}/Sm^{3+} which has a $E^{0'}$ of 1.311 V vs $E_{Li/Li(I)}{}^{0'}$ [35].

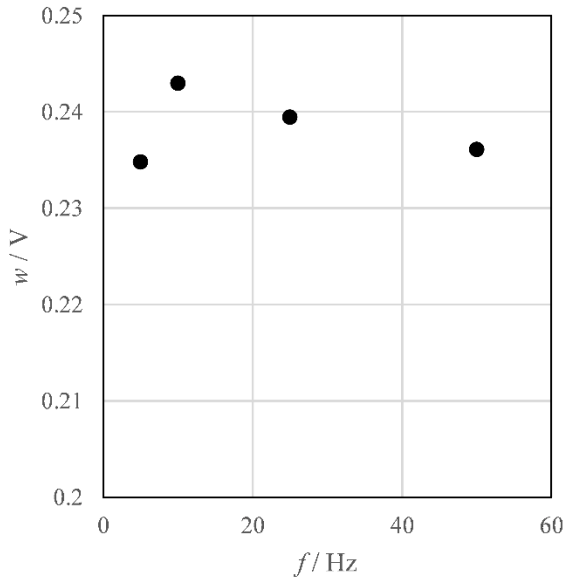

Figure 10. *w* vs *f* from *iR*-compensated square-wave voltammograms of the soluble/soluble reaction in System 3. A = 0.718 cm^2, ΔE_s = 5 mV, ΔE_{sw} = 20 mV, R_u = 0.028 Ω.

Next, CV data was taken with a E_{step} of 1 mV and Equation 3 was applied to the data in Figure 11. The differential height method was used to estimate that A = 0.718 cm^2, a $D_{Sm(II)/Sm(III)}$ value was taken from literature to be 0.654 x 10^{-5} cm^2 s^{-1} [36], and the unknown analyte was concluded to be 0.041 ± 0.004 M $SmCl_3$ (0.114 ± 0.010 mol% or 0.525 ± 0.048 wt%). For a rough concentration calculation, this compares well with the pre-measured analyte concentration (0.71 wt%) with an error of 26.1%.

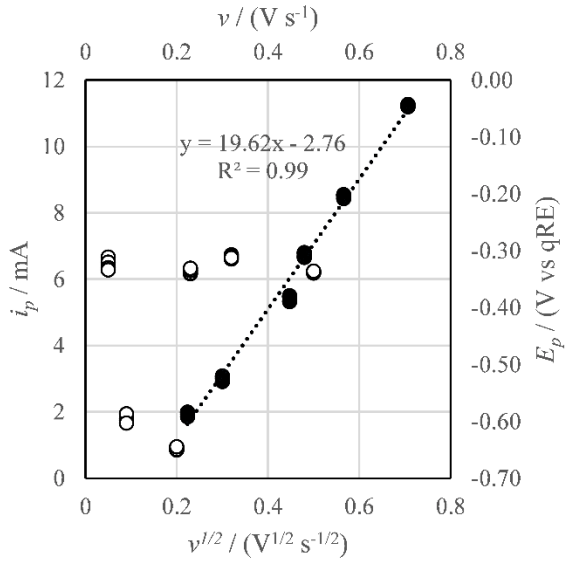

Figure 11. i_p vs $v^{1/2}$ (filled) and E_p vs v (empty). A = 0.718 cm^2, ΔE_{step} = 1 mV, R_u = 0.028 Ω.

3.5 System 4 Identification. A full-window, *iR*-compensated CV scan was taken of System 4 which revealed ~11 electrochemical reactions. Following the full window scan, the upper and lower potential limits were adjusted to investigate the connections between different peaks (see Figures 12 and 13). Peaks B, B', B", C, D, D', D", E, E', F, F', G, G', H, and H' were classified as belonging to the analytes. A/A' and I'/I were classified as belonging to Li^+ reduction to Li and Cl^- oxidation to Cl_2, respectively. During these measurements, it was revealed that D" only was present in a scan if D occurred; likewise with B" and B. These dependencies indicated shared reactants and/or products between the reactions.

This is an Accepted Manuscript of an article published by Taylor & Francis in Nuclear Technology on June 12, 2024, available at: https://doi.org/10.1080/00295450.2024.2348849.

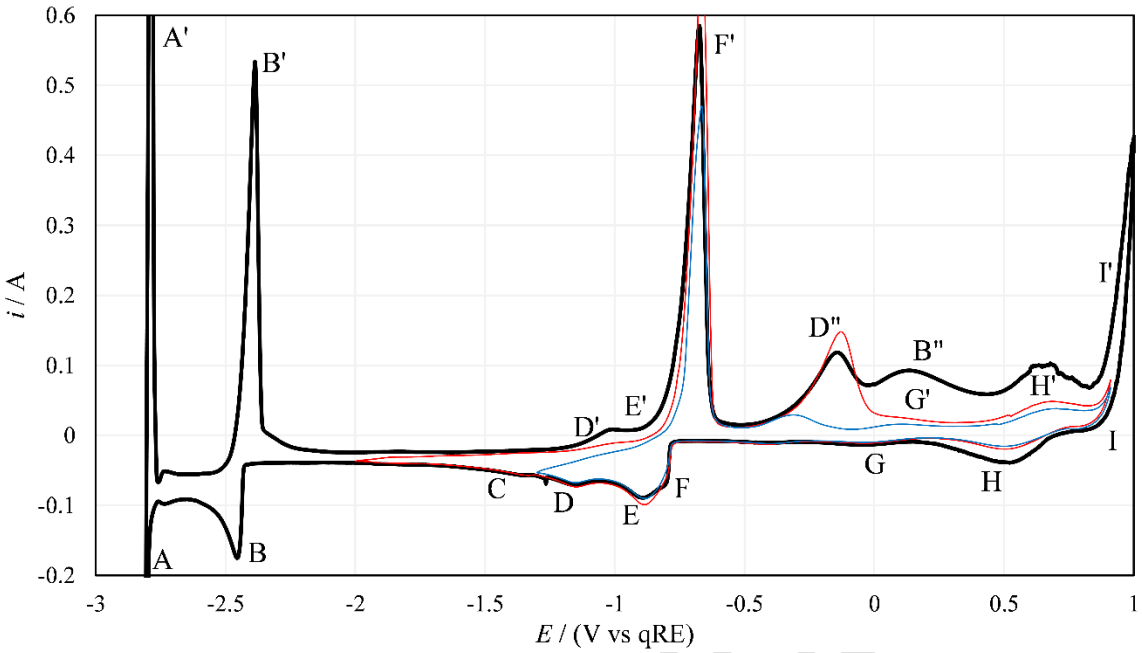

Figure 12. *iR*-compensated cyclic voltammograms of System 4 with varying potential ranges, including a full window scan (thick black). A = 0.523 cm^2, v = 300 mV s^{-1}, E_{step} = 1 mV, R_u = 0.043 Ω.

3.5.1 Identification of Species. The investigation began by stepping the positive and negative switching potentials towards the center of the voltammogram (see Figures 12 and 13) to find relationships between different reactions. For instance, D" only appeared when the negative switching potential was set up to or beyond D (compare blue and red curves in bottom plot of Figure 13), and B" only occurred when the negative switching potential was set beyond B. With the information gathered, peaks B, G', H', and D were selected as the best candidates for quantitative analysis. Peak C was presumed to be associated with impurities, interactions, or adsorption due to its small size and lack of corresponding oxidation peak. Peak J (-0.4 V vs qRE) was ignored because it had no apparent coupled oxidation peak and could simply be the adsorption of a species responsible for peak F, as has been observed for U deposition [37–39].

This is an Accepted Manuscript of an article published by Taylor & Francis in Nuclear Technology on June 12, 2024, available at: https://doi.org/10.1080/00295450.2024.2348849.

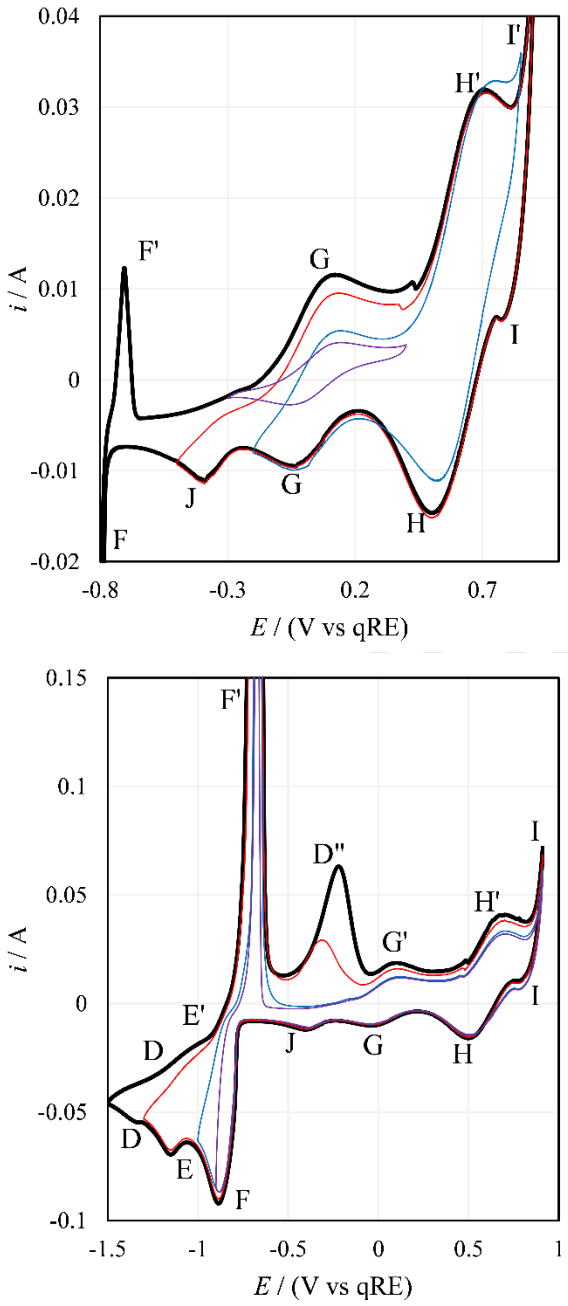

Figure 13. *iR*-compensated cyclic voltammograms of System 4. Scans with relatively narrow (top) and wide (bottom) potential ranges. A = 0.523 cm^2, v = 300 mV s^{-1}, E_{step} = 1 mV, R_u = 0.043 Ω.

The onset of B with cyclic voltammetry was used to estimate $E_B^{0'}$ to be 0.341 V vs Li$^+$/Li. This value is only an estimation however due to the possibility of underpotential deposition. SWV and Equation 2 were used to estimate that n_B = 1.4. However, only limited confidence was placed in this value

because significant WE area growth may have occurred during the measurement and only one *f* was used during SWV. Peaks B/B' occurred at a potential much more negative ($\Delta E_p \approx$ -1.5 V) than peaks F/F', which has behavior characteristic of soluble-insoluble reactions (i.e., deposition). SWV was performed at 5 Hz and a step potential of -3 mV. Hence, the time elapsed between peak B and F was ~100 seconds in the SWV measurement. During this time, deposits are constantly forming on the electrode from the reaction associated with peak F. Evidence for surface area growth was the tail of Peak B in SWV measurement not returning to background levels. Fuller et al. [15] noted that SWV peaks broaden due to deposits augmenting the surface area, which in turns decreases the estimated *n* (see Equation 2). Hence, it was suspected that *n* would underestimated based on the SWV data. If the analyte was $MgCl_2$, $n = 2$ could be valid, but the Mg-Li alloy peak observed in System 1 (see Figure 1) was not present in this system [26,40]. A reaction with $n = 1$ is also unlikely because there is no known $n = 1$ reaction close to $E_B^{0'}$. This left possible reactants of Nd^{3+}, Gd^{3+}, or La^{3+}, and La^{3+} reduction to La was selected as the likely choice based on its tabulated redox potential of 0.427 V vs Li^+/Li [13]. This selection was verified by using Equation 4 and a stand-in D_j value of 10^{-5} cm^2 s^{-1} to calculate an approximate C_O^* value which was then used with Equation 5 to estimate a $E_B^{0'}$ value of 0.464 V vs Li^+/Li (only a difference of 37 mV, see Table 2). Based on this information, the analyte responsible for B was identified as $LaCl_3$ because it has the most negative reduction potential of the lanthanide series.

G' and H' were next analyzed using SWV and semi-differentiated CV data (see Figure 14). Equation 1 and the SWV data estimated that $n = 1$ for both G' and H'. $E^{0'}$ for G' and H' was estimated by assuming that the *D* values of the reduced and oxidized species were equal for G/G' and H/H'. With that assumption, the peak potential of semi-differentiated CV data is theoretically equal to $E^{0'}$ [20]. Therefore, $E^{0'}$ (or E_p) was calculated to be 2.723 V vs Li^+/Li and 3.299 V vs Li^+/Li for G' and H', respectively. This was sufficient information for the analyte responsible for G' to be identified as Cr^{2+}, however this information was not sufficient to identify the analyte responsible for H' because both Cu^+ and Fe^{2+} were likely candidates.

This is an Accepted Manuscript of an article published by Taylor & Francis in Nuclear Technology on June 12, 2024, available at: https://doi.org/10.1080/00295450.2024.2348849.

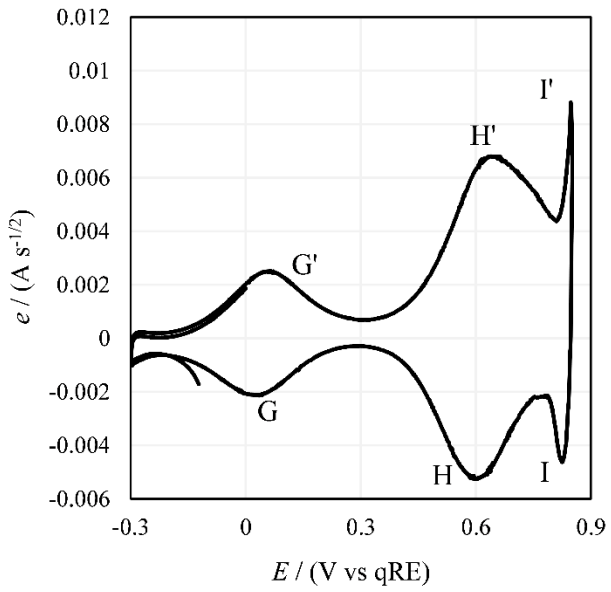

Figure 14. Semi-differentiated CV data for peaks G', H', G, and G. A = 0.523 cm^2, v = 50 mV s^{-1}, ΔE_{step} = 1 mV, R_u = 0.043 Ω.

Peaks F, E, and D were then analyzed because their redox potentials lay approximately where the reductions for Cr^{2+}, Fe^{2+}, or Cu^{+} (candidate products for H and G) occurred. Peak F, which displayed a typical soluble-insoluble shape was analyzed using the semi-differentiated, soluble-insoluble relations (Equations 8-10). This signal was then subtracted from the overall semi-derivate which then revealed that the shape of semi-differentiated peaks for E and D were typical of soluble-soluble reactions (see Figure 15).

$E^{0'}$ for the reaction associated with peak F was calculated using two methods. First, C_O^* was estimated by using D_O = 10^{-5} cm^2 s^{-1}, Equation 9, and $e(E_{1/2})$ of -0.0758 A s$^{0.5}$ for Peak F in Figure 15. This C_O^* value (3.16 mol cm^{-3}) was then used with Equation 5 to estimate that $E^{0'}$ = 1.932 V vs Li$^+$/Li. Second, the semi-derivative's peak potential was assumed to be approximately $E_{1/2}$ and Equation 9 was used to estimate that $E^{0'}$ = 1.944 V vs Li$^+$/Li. Based on these potentials, it became clear that peak F was likely Fe^{2+} reduction to Fe ($E^{o'}$ = 2.132 V) because the reduction of Cu^+ to Cu ($E^{o'}$ = 2.347) was substantially more positive. Therefore, the analyte responsible for peak F and H' was assumed to be Fe^{2+}.

This is an Accepted Manuscript of an article published by Taylor & Francis in Nuclear Technology on June 12, 2024, available at: https://doi.org/10.1080/00295450.2024.2348849.

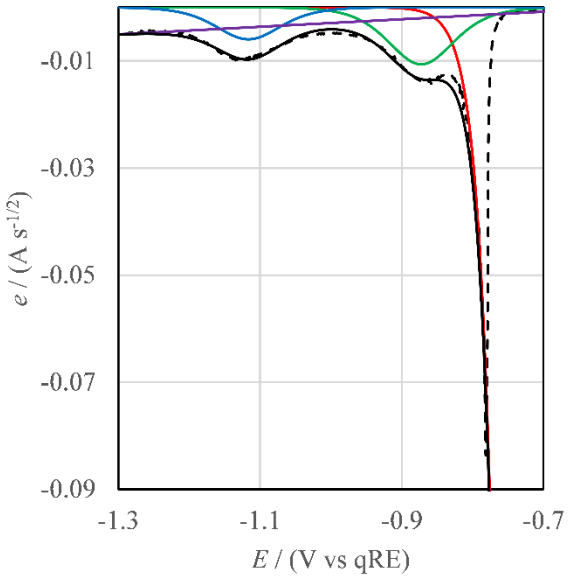

Figure 15. Semi-differentiated CV data for peaks F, E, and D. A = 0.523 cm^2, v = 50 mV s^{-1}, ΔE_{step} = 1 mV, R_u = 0.043 Ω. Semi-differentiated data (dotted black), fitted baseline (purple), fitted soluble/insoluble curve (red), fitted soluble/soluble curves (green and blue), summation of the fitted models (solid black).

Following this analysis, peaks D and E remained to be identified. The redox potential of peak E made the reduction of Cr^{2+} to Cr (soluble-insoluble) a possibility, but the apparent soluble-soluble form of its e vs E curve was initially puzzling because the soluble-soluble semi-differentiated relations could be fitted to them so well (see Figure 15). However, an analogous La-Gd system where typical soluble-soluble voltammetry behavior has been observed in solid solutions made this behavior plausible [41]. According to the Fe-Cr phase diagram, Cr is appreciably soluble (~18 mol%) in solid Fe at 773 K before a two-phase region occurs [42]. Therefore, peak E was attributed to Cr^{2+} reduction to Cr into Fe. This attribution was confirmed by calculating that the n value for peak E was 1.74, using the width of at half height for the e vs E curve and Equation 1 which holds for both SWV and semi-differentiated CV in reversible, soluble-soluble reactions [20].

Peak D also displays the typical shape of a soluble-soluble reaction and the width of the SWV peak indicated that n = 2. The estimated $E^{0'}$ value of 1.549 V vs Li^+/Li indicates that this could be Zr^{4+}

reduction to Zr^{2+}, but the lack of a Zr^{2+} reduction peak to Zr indicates that Zr^{4+} is not the responsible analyte. Based on the approximate $E^{0'}$ value, the reduction of Sm^{3+} to Sm^{2+} is possible, despite inconsistencies in the value of *n*. However, the dependence of D' on the reactions associated with B indicated that D may just be associated with alloy or intermetallic formation (see the difference in D' between the scan represented by the black line and scan represented by the red line in Figure 12). With this information and no additional experimental data to give clarity, it was assumed that $SmCl_3$ was the analyte responsible for peak D and that peaks C, D", and B" were results of adsorption, desorption, alloys, or intermetallics.

3.5.2 Quantification of Species. After analyte identity guesses of $LaCl_3$, $CrCl_3$, $FeCl_2$, and $SmCl_3$ were finalized, but before they were quantified, it was revealed that only that $LaCl_3$, $CrCl_3$, and $FeCl_2$ were present; $SmCl_3$ was not present in the sample. This marked an exception in the study because the analytes in all the other systems were identified and quantified before any information about the system was revealed.

To begin quantification, *A* was approximated to be 0.523 cm^2 using the differential height method. Then, peak B was analyzed using CV data that had a linear i_p vs $v^{1/2}$ plot (see Figure 16), a $D_{La(III)}$ value of 2.03 x 10^{-5} cm^2 s^{-1} from literature [43] and Equation 4. It was then concluded that the analyte responsible for peak B was 0.79 wt% $LaCl_3$ (52.5 mM). This corresponds to an error of 20.8% when compared to the weighed value of 0.998 wt% $LaCl_3$.

This is an Accepted Manuscript of an article published by Taylor & Francis in Nuclear Technology on June 12, 2024, available at: https://doi.org/10.1080/00295450.2024.2348849.

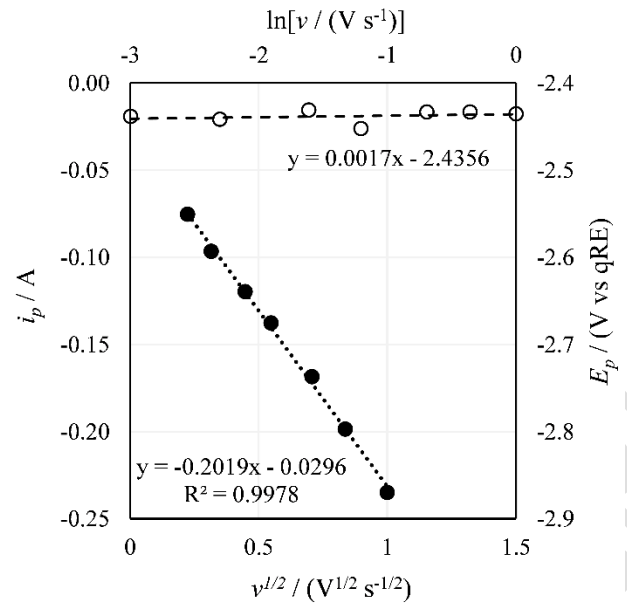

Figure 16. i_p vs $v^{1/2}$ (closed circles) and E_p vs $ln(v)$ (open circles) for Peak B.

A similar method was used for peak G', however a $D_{Cr(II)}$ value of 1.67 x 10^{-5} cm^2 s^{-1} [44] and Equation 3 were used (see Figure 17). This indicated that $C_{Cr(II)}^*$ was 45.7 mM, however $C_{Cr}^* = C_{Cr(II)}^* + C_{Cr(III)}^*$. Therefore, the OCP was used to estimate the ratio of $C_{Cr(III)}^*$ to $C_{Cr(II)}^*$. Using this reasoning, OCP, and $E^{0'}$ values, molar ratios of 0.311 for Cr^{3+}/Cr^{2+} and 5.5 × 10^{-5} for Fe^{3+}/Fe^{2+} were calculated.

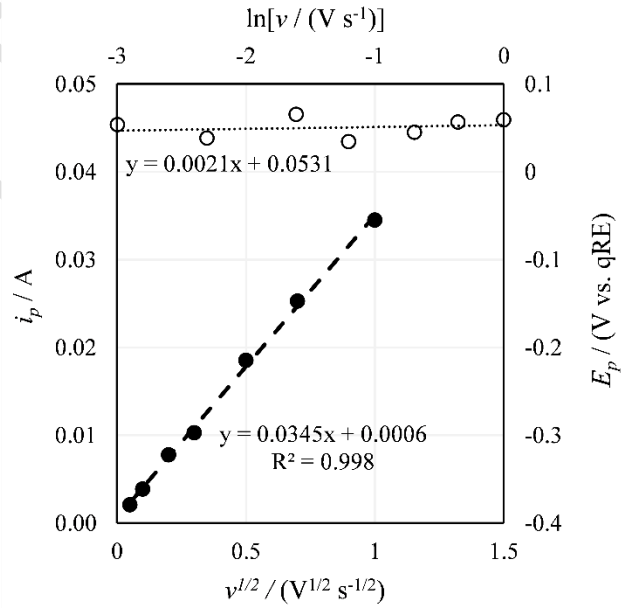

Figure 17. i_p vs $v^{1/2}$ (closed circles) and E_p vs $ln(v)$ (open circles) for Peak G'.

This is an Accepted Manuscript of an article published by Taylor & Francis in Nuclear Technology on June 12, 2024, available at: https://doi.org/10.1080/00295450.2024.2348849.

Hence, at equilibrium, Fe is assumed to be only present as Fe^{2+}, while Cr is present in both the Cr^{3+} and Cr^{2+} states. With this information, C_{Cr}^{*} was calculated to be 59.9 mM (0.586 wt% if added as $CrCl_3$). This corresponds to 101.3% error when compared to the pre-measured value of 0.291 wt%. Peak H' used the same methods (see Figure 18), a $D_{Fe(II)}$ value of 2.16 x 10^{-5} cm^2 s^{-1} [45,46], and calculated that C_{Fe}^{*} was 0.59 wt% (75.8 mM). This corresponds to 10.7% error when compared to the pre-measured value of 0.533 wt%.

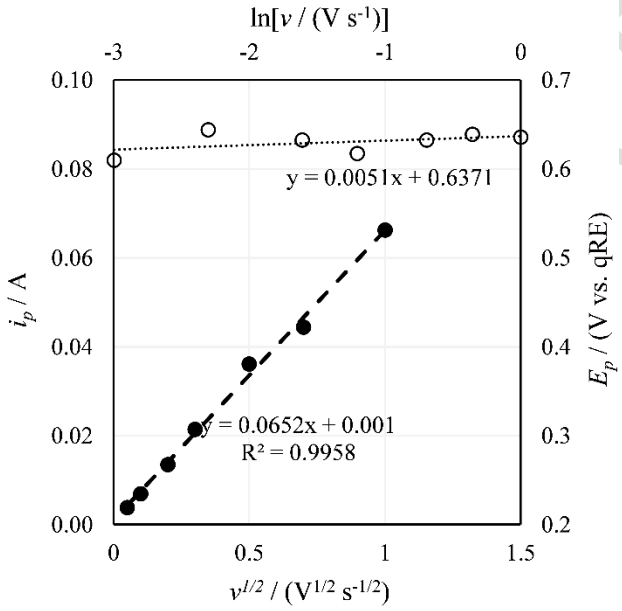

Figure 18. i_p vs $v^{1/2}$ (closed circles) and E_p vs $ln(v)$ (open circles) for Peak H'.

4. Discussion

After identity and quantity was determined (with an aforementioned caveat for System 4), the identities and concentrations of guesses were compared to the prepared solutions in Table 4. Without exception, every analyte placed in their solution was positively identified. However, System 4 included a false positive of $SmCl_3$ because an interaction between the three other analytes was mistakenly attributed to $SmCl_3$. On the other hand, quantification accuracy was typically within an order of magnitude, with the exception of System 2 (i.e., VCl_3). It should be restated that the focus of this study was on identification, not quantification, of unknown analytes. Therefore, the prepared concentrations only refer to the mass of

analyte measured out into the crucible before melting the solution in a furnace. No analytical quantification of analytes (besides rough electrochemical measurements shown above) was made during or after the experiment to determine the true concentration of analyte. In future work, three objectives seem apparent: (1) pushing the ability to identify species in ever more complex, interfering environments, (2) increasing the accuracy of quantitative predictions of blind samples, and (3) investigating the use of algorithms or artificial intelligences as an alternative means of interpreting electroanalytical data.

Table 4. Overall results of the detection of analytes without prior system knowledge.

System	Guessed Identity	True Identity	Guessed Concentration / wt%	Prepared Concentration / wt%
1	$MgCl_2$	$MgCl_2$	0.574	0.708
2	VCl_3	VCl_3	0.313	2.66
3	$SmCl_3$	$SmCl_3$	0.525	0.71
4	$SmCl_3$	not present	-	-
4	$LaCl_3$	$LaCl_3$	0.79	0.998
4	$CrCl_3$	$CrCl_3$	0.586	0.291
4	$FeCl_2$	$FeCl_2$	0.59	0.533

The two least accurate quantitative concentration predictions were made in the VCl_3 system (System 2) and the $CrCl_3$ prediction in the $LaCl_3$-$CrCl_3$-$FeCl_2$ system (System 4). While every analysis included some technical errors and published diffusion coefficients could contain significant errors, a brief explanation is given for these two least accurate predictions. The error in System 2 seems to be a function of the volatility of VCl_3. Therefore, the concentration at the time of measurement may have been closer to their guessed value. Error in System 4 may have been due to underestimated diffusion

coefficient value, inaccurate estimate of the molar ratio of Cr^{3+}/Cr^{2+}, significant background currents, and/or chemical reactions occurring alongside the electrochemical as the La, Cr, and Fe ions interacted with one another. Due to the exponential relationship between the molar ratio and potential in Equation 5, even slight inaccuracies in the estimation of the OCP and $E^{o'}$ could be magnified to introduce significant error. We suspect that the Cr prediction was least accurate in System 4 because its Cr^{3+}/Cr^{2+} signal lay between the signal for the other two species that were present. In the complex melt, there was evidence that the added $CrCl_3$ reacted to some extent to results in both Cr^{2+} and Cr^{3+} being present in the bulk solution. There may have been multiple chemical and electrochemical interactions impacting the Cr^{2+}/Cr^{3+} signal.

The false positive of $SmCl_3$ in System 4 highlights the need to explore and understand the signals that may arise due to interaction of actinide and fission product elements in the molten salts more fully. System 4 shows that unexpected chemical interactions can result in false positives. More studies are needed to identify additional signals that may arise as fission and corrosion products grow into MSR salt, ER salt or other process salts. Without confirming the presence or absences of signals from interactions in the vicinity of actinide signals, an electrochemical sensor could be "spoofed" into indicating or overestimating the presence of nuclear material within a process.

Lastly, these experiments were conducted by individuals who used their experience and judgement to discern which signals were related to the analyte and which signals were attributed to background/impurities. This introduced variability in the study due to human behavior, especially in the tendency to dismiss electrochemical signals as being associated with background, impurities, or interactions. Despite these issues, we observed that human judgement and discernment based on experience served the electrochemists in this study well, helping them accurately identify analytes. Perhaps, an automated algorithm or artificial intelligence could be developed to help facilitate more impartial and consistent analysis of electrochemical signals. However, it should be noted that any such

program would not be completely free from bias [12], would require a careful filtering of the literature to only use high quality training data [24], and should be frequently verified by competent human analysts.

5. Conclusion

To evaluate the electroanalytical methods available for molten salt systems in the present day, unknown metal chloride analytes were identified in eutectic LiCl-KCl. The most useful methods for identification included: (1) the estimation of $E^{0'}$ values using OCP and Nernst equation or voltammetry peaks and their associated relations and (2) varying CV windows to find relationships between reduction and oxidation signals. Every analyte placed in solutions were positively identified, however there was one false-positive. Quantitative predictions of the unknown analytes were also made which were accurate within a factor of two (with one exception of System 2). However, ICP-MS analysis of the salts was not performed post-measurement to validate their quantitative predictions because the focus of the study was on the identification of the unknown analyte. Hence, these errors may be overpredicted due to a loss of salt due to volatilization and/or formation and precipitation of oxides. For some analyte combinations, a significant number of additional signals appear due to interaction of the ions and deposits which resulted in the false-positive of Sm^{3+}. This study highlights the need to further study the interactions between important actinide, fission product, and corrosion product ions and deposits to improve the accuracy of electrochemical sensors in nuclear material accounting applications.

References

[1] Bureau of International Safeguards and Nonproliferation, Declaration to Triple Nuclear Energy, U. S. Dep. State (2023). https://www.state.gov/declaration-to-triple-nuclear-energy/ (accessed December 22, 2023).

[2] Office of the Spokesperson, The United States Joins Multinational Declaration to Triple Nuclear Energy Capacity by 2050 to Support Global Climate and Energy Security Goals, U. S. Dep. State (2023). https://www.state.gov/the-united-states-joins-multinational-declaration-to-triple-nuclear-energy-capacity-by-2050-to-support-global-climate-and-energy-security-goals/ (accessed December 22, 2023).

[3] International Atomic Energy Agency (IAEA), Advanced Reactor Information System (AIRS), (n.d.). https://aris.iaea.org/sites/overview.html (accessed February 5, 2021).

[4] G.L. Fredrickson, M.N. Patterson, D. Vaden, G.G. Galbreth, T.-S. Yoo, J.C. Price, E.J. Flynn, R.N. Searle, History and status of spent fuel treatment at the INL Fuel Conditioning Facility, Prog. Nucl. Energy 143 (2022) 104037. https://doi.org/10.1016/j.pnucene.2021.104037.

[5] T. Williams, R. Shum, D. Rappleye, Review—Concentration Measurements In Molten Chloride Salts Using Electrochemical Methods, J. Electrochem. Soc. 168 (2021) 123510. https://doi.org/10.1149/1945-7111/ac436a.

[6] R.G. Lewin, M.T. Harrison, 15 - International developments in electrorefining technologies for pyrochemical processing of spent nuclear fuels, in: R. Taylor (Ed.), Reprocess. Recycl. Spent Nucl. Fuel, Woodhead Publishing, Oxford, 2015: pp. 373–413. https://doi.org/10.1016/B978-1-78242-212-9.00015-0.

[7] J. Serp, M. Allibert, O. Beneš, S. Delpech, O. Feynberg, V. Ghetta, D. Heuer, D. Holcomb, V. Ignatiev, J.L. Kloosterman, L. Luzzi, E. Merle-Lucotte, J. Uhlíř, R. Yoshioka, D. Zhimin, The molten salt reactor (MSR) in generation IV: Overview and perspectives, Prog. Nucl. Energy 77 (2014) 308–319. https://doi.org/10.1016/j.pnucene.2014.02.014.

[8] D. Zhang, L. Liu, M. Liu, R. Xu, C. Gong, J. Zhang, C. Wang, S. Qiu, G. Su, Review of conceptual design and fundamental research of molten salt reactors in China, Int. J. Energy Res. 42 (2018) 1834–1848. https://doi.org/10.1002/er.3979.

[9] J. Zhang, Electrochemistry of actinides and fission products in molten salts—Data review, J. Nucl. Mater. 447 (2014) 271–284. https://doi.org/10.1016/j.jnucmat.2013.12.017.

[10] P. Wang, A. Leong, J. Zhang, Electrochemical Methods for Fundamental Data Measurements in Molten Salts, JOM 75 (2023) 3687–3698. https://doi.org/10.1007/s11837-023-05931-2.

[11] G.M. Haarberg, J. Thonstad, Electrochemical properties of metal-molten salt mixtures, J. Appl. Electrochem. 19 (1989) 789–801. https://doi.org/10.1007/BF01007924.

[12] I.E. Dror, Cognitive and Human Factors in Expert Decision Making: Six Fallacies and the Eight Sources of Bias, Anal. Chem. 92 (2020) 7998–8004. https://doi.org/10.1021/acs.analchem.0c00704.

[13] J.A. Plambeck, Electromotive force series in molten salts, J. Chem. Eng. Data 12 (1967) 77–82. https://doi.org/10.1021/je60032a023.

[14] C. Caravaca, G.D. Córdoba, Formation of Gd-Al Alloy Films by a Molten Salt Electrochemical Process, Z. Für Naturforschung A 63 (2008) 98–106. https://doi.org/10.1515/zna-2008-1-217.

[15] R. Fuller, T. Williams, M. Schvaneveldt, D. Rappleye, A Comparison of Square-Wave Voltammetry Models to Determine the Number of Electrons Exchanged in Metal Deposition, Electrochimica Acta (2022) 140220. https://doi.org/10.1016/j.electacta.2022.140220.

[16] T. Berzins, P. Delahay, Oscillographic Polarographic Waves for the Reversible Deposition of Metals on Solid Electrodes, J. Am. Chem. Soc. 75 (1953) 555–559. https://doi.org/10.1021/ja01099a013.

[17] J.E.B. Randles, A cathode ray polarograph. Part II.—The current-voltage curves, Trans. Faraday Soc. 44 (1948) 327–338. https://doi.org/10.1039/TF9484400327.

[18] A. Ševčík, Oscillographic polarography with periodical triangular voltage, Collect. Czechoslov. Chem. Commun. 13 (1948) 349–377. https://doi.org/10.1135/cccc19480349.

[19] W. Nernst, Die elektromotorische Wirksamkeit der Jonen, Z. Für Phys. Chem. 4U (1889) 129–181. https://doi.org/10.1515/zpch-1889-0412.
[20] P. Dalrymple-Alford, M. Goto, K.B. Oldham, Shapes of derivative neopolarograms, J. Electroanal. Chem. Interfacial Electrochem. 85 (1977) 1–15. https://doi.org/10.1016/S0022-0728(77)80148-4.
[21] M.M. Tylka, J.L. Willit, J. Prakash, M.A. Williamson, Application of Voltammetry for Quantitative Analysis of Actinides in Molten Salts, J. Electrochem. Soc. 162 (2015) H852. https://doi.org/10.1149/2.0281512jes.
[22] T. Williams, R. Fuller, C. Vann, D. Rappleye, Semi-Differentiation of Reversible, Soluble-Insoluble Potential Sweep Voltammograms, J. Electrochem. Soc. 170 (2023) 042502. https://doi.org/10.1149/1945-7111/accc59.
[23] N. Fatouros, D. Krulic, H. Groult, Linear sweep and staircase voltammetries for reversible deposition of metal ions on the same metal and on foreign substrates, J. Electroanal. Chem. 625 (2009) 1–6. https://doi.org/10.1016/j.jelechem.2008.07.028.
[24] D. Rappleye, R. Fuller, Bringing the Analysis of Electrodeposition Signals in Voltammetry Out of the Shadows, J. Electrochem. Soc. (2023). https://doi.org/10.1149/1945-7111/acd879.
[25] G.J. Janz, R.P.T. Tomkins, C.B. Allen, J.R. Downey Jr., G.L. Garner, U. Krebs, S.K. Singer, Molten salts: Volume 4, part 2, chlorides and mixtures—electrical conductance, density, viscosity, and surface tension data, J. Phys. Chem. Ref. Data 4 (1975) 871–1178. https://doi.org/10.1063/1.555527.
[26] A.M. Martínez, B. Børresen, G.M. Haarberg, Y. Castrillejo, R. Tunold, Electrodeposition of magnesium from the eutectic LiCl–KCl melt, J. Appl. Electrochem. 34 (2004) 1271–1278. https://doi.org/10.1007/s10800-004-1761-6.
[27] T. Støre, G.M. Haarberg, R. Tunold, Determination of diffusion coefficients of depositing ions in molten chlorides by transient electrochemical techniques, J. Appl. Electrochem. 30 (2000) 1351–1360. https://doi.org/10.1023/A:1026578713427.
[28] N. Fatouros, D. Krulic, Analysis of the square wave voltammetry for reversible metal deposition on a foreign substrate – Experimental study of silver deposition on gold, J. Electroanal. Chem. 706 (2013) 76–85. https://doi.org/10.1016/j.jelechem.2013.07.019.
[29] D. Shen, R. Akolkar, Electrodeposition of Neodymium from NdCl3-Containing Eutectic LiCl–KCl Melts Investigated Using Voltammetry and Diffusion-Reaction Modeling, J. Electrochem. Soc. 164 (2017) H5292. https://doi.org/10.1149/2.0451708jes.
[30] D. Rappleye, D. Horvath, Z. Wang, C. Zhang, M.F. Simpson, Methods for Determining the Working Electrode Interfacial Area for Electroanalytical Measurements of Metal Ions in Molten LiCl-KCl, ECS Trans. 75 (2016) 79. https://doi.org/10.1149/07515.0079ecst.
[31] R. Yuan, C. Lv, H. Wan, S. Li, Y. Che, Y. Shu, J. He, J. Song, Electrochemical behavior of vanadium ions in molten LiCl-KCl, J. Electroanal. Chem. 891 (2021) 115259. https://doi.org/10.1016/j.jelechem.2021.115259.
[32] I.B. Polovov, M.E. Tray, M.V. Chernyshov, V.A. Volkovich, B.D. Vasin, O.I. Rebrin, Electrode Processes in Vanadium-Containing Chloride Melts, in: Molten Salts Chem. Technol., John Wiley & Sons, Ltd, 2014: pp. 257–281. https://doi.org/10.1002/9781118448847.ch4e.
[33] C. Amatore, C. Lefrou, F. Pflüger, On-line compensation of ohmic drop in submicrosecond time resolved cyclic voltammetry at ultramicroelectrodes, J. Electroanal. Chem. Interfacial Electrochem. 270 (1989) 43–59. https://doi.org/10.1016/0022-0728(89)85027-2.
[34] C. Amatore, E. Maisonhaute, G. Simonneau, Ohmic drop compensation in cyclic voltammetry at scan rates in the megavolt per second range: access to nanometric diffusion layers via transient electrochemistry, J. Electroanal. Chem. 486 (2000) 141–155. https://doi.org/10.1016/S0022-0728(00)00131-5.
[35] Y. Castrillejo, C. de la Fuente, M. Vega, F. de la Rosa, R. Pardo, E. Barrado, Cathodic behaviour and oxoacidity reactions of samarium (III) in two molten chlorides with different acidity properties: The eutectic LiCl–KCl and the equimolar CaCl2–NaCl melt, Electrochimica Acta 97 (2013) 120–131. https://doi.org/10.1016/j.electacta.2013.02.115.

[36] H. Andrews, S. Phongikaroon, Development of an Experimental Routine for Electrochemical and Laser-Induced Breakdown Spectroscopy Composition Measurements of SmCl3 in LiCl-KCl Eutectic Salt Systems, Nucl. Technol. 205 (2019) 891–904. https://doi.org/10.1080/00295450.2018.1551988.
[37] D. Rappleye, K. Teaford, M. Simpson, Investigation of the Effects of Uranium(III)-Chloride Concentration on Voltammetry in Molten LiCl-KCl Eutectic with a Glass-Tungsten Fused Electrode, Electrochimica Acta 219 (2016) 721–733. https://doi.org/10.1016/j.electacta.2016.10.075.
[38] M.M. Tylka, J.L. Willit, J. Prakash, M.A. Williamson, Method Development for Quantitative Analysis of Actinides in Molten Salts, J. Electrochem. Soc. 162 (2015) H625–H633. https://doi.org/10.1149/2.0401509jes.
[39] K. Serrano, P. Taxil, Electrochemical reduction of trivalent uranium ions in molten chlorides, J. Appl. Electrochem. 29 (1999) 497–503. https://doi.org/10.1023/A:1003402029895.
[40] D. Rappleye, M.L. Newton, C. Zhang, M.F. Simpson, Electroanalytical measurements of binary-analyte mixtures in molten LiCl-KCl eutectic: Uranium(III)- and Magnesium(II)-Chloride, J. Nucl. Mater. 486 (2017) 369–380. https://doi.org/10.1016/j.jnucmat.2017.01.047.
[41] D. Rappleye, S.-M. Jeong, M. Simpson, Electroanalytical Measurements of Binary-Analyte Mixtures in Molten LiCl-KCl Eutectic: Gadolinium(III)- and Lanthanum(III)-Chloride, J. Electrochem. Soc. 163 (2016) B507–B516. https://doi.org/10.1149/2.1011609jes.
[42] S.-L. Chen, J.-Y. Zhang, X.-G. Lu, K.-C. Chou, Y.A. Chang, Application of Graham scan algorithm in binary phase diagram calculation, J. Phase Equilibria Diffus. 27 (2006) 121–125. https://doi.org/10.1007/s11669-006-0034-y.
[43] F. Lantelme, Y. Berghoute, Electrochemical Studies of LaCl3 and GdCl3 Dissolved in Fused LiCl-KCl, J. Electrochem. Soc. 146 (1999) 4137. https://doi.org/10.1149/1.1392604.
[44] F. Lantelme, K. Benslimane, M. Chemla, Electrochemical properties of solutions of CrCl2 and CrCl3 in molten alkali chlorides, J. Electroanal. Chem. 337 (1992) 325–335. https://doi.org/10.1016/0022-0728(92)80545-F.
[45] D. Inman, J.C. Legey, R. Spencer, I. A chronopotentiometric study of iron in LiCl-KCl, J. Appl. Electrochem. 8 (1978) 269–272. https://doi.org/10.1007/BF00616430.
[46] A. Lugovskoy, M. Zinigrad, D. Aurbach, Electrochemical Determination of Diffusion Coefficients of Iron (II) Ions in Chloride Melts at 700-750°C, Isr. J. Chem. 47 (2007) 409–414. https://doi.org/10.1560/IJC.47.3-4.409.